ESS515/415

Magnetic Field Reconnection
(aka magnetic field annihilation)

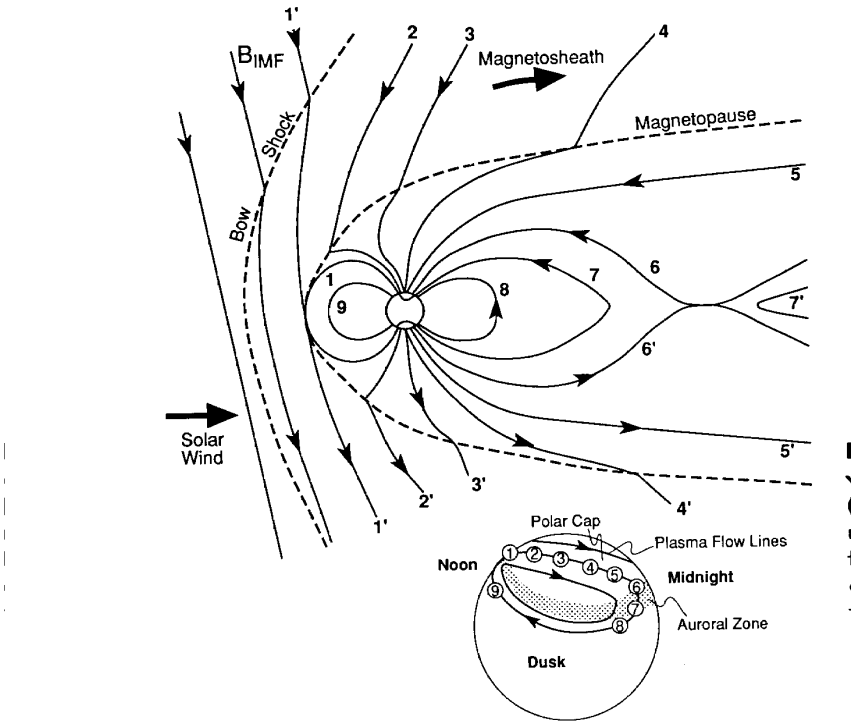

In 1961 Dungey proposed a process whereby the magnetic field in the interplanetary medium could be made to directly connect with the earth's magnetic field. The first analytic analysis of this was presented by Sweet and Parker for a conducting fluid. As it turned out, the Sweet/Parker model of Reconnection is too slow, and it was not until the Petcheck model was presented that the idea of magnetic reconnnection started to become a unifying theory for understanding the magnetosphere. In this process the entire magnetosphere is put in motion, as illustrated in this diagram (From Kivelson and Russell, 1995). The interplanetary magnetic field line B_{IMF} connects with the earth's field at 1 and is dragged back across the magnetosphere 1 - 5 and 1' - 5', where it closes the cycle with a pinching off of the field at 6/6' allowing field line 7 to snap back toward the earth and 7' to head onward radially away from the sun.

The next 4 pages are from Kivelson and Russell which describes the simple fluid version of reconnection. Following that are several figures with data to support the idea.

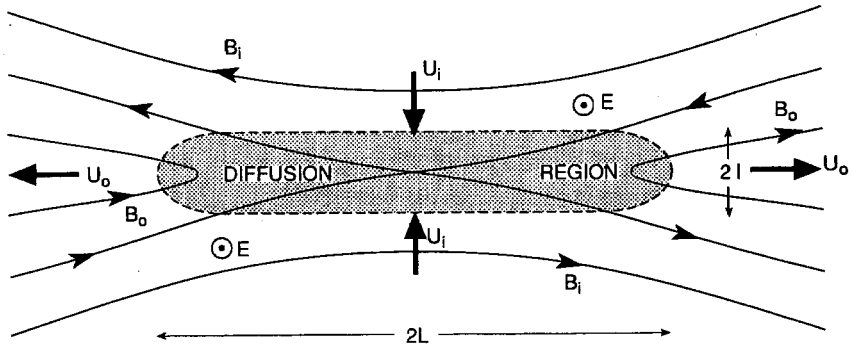

FIG. 9.12. Sweet-Parker reconnection geometry, in which all the reconnecting plasma flows through the shaded diffusion region. Very slow reconnection results.

Part of the reason that the Dungey model took so long to be accepted was that magnetic reconnection was poorly understood as a physical process. In the next two sections we shall examine reconnection from a fluid or MHD perspective and then from a particle-motion viewpoint and show that the two descriptions are equivalent. We shall then return to the magnetopause and tail and examine their more detailed morphology in the light of reconnection theory.

9.4.3 Fluid Descriptions of Reconnection

In this section we follow the development of MHD fluid descriptions of magnetic reconnection. The models will be time-stationary and two-dimensional. The main concern will be to establish that reconnection can proceed fast enough for it to have an effect in space-plasma systems. We find that it can, but only when the plasma far from the diffusion region adjusts to the new flow pattern.

We start with the Sweet-Parker solution shown in Figure 9.12. This is a basic x-line configuration introduced in Figure 9.10. The diffusion region, shown shaded, is $2L$ long and $2l$ wide, where $L \gg l$. For simplicity, we assume that the inflow and outflow regions (parameters that are identified by subscripts i and o) are symmetrical. This is appropriate for reconnection in the tail, where the inflowing plasma comes from the northern and southern lobes. At the magnetopause, the two inflow regions are quite different, as we discuss in Section 9.5. As before, the electric field E is spatially uniform and points out of the page, so that

$$E = u_i B_i = u_o B_o \tag{9.28}$$

We further assume that the flow is incompressible, that is, $\rho_i = \rho_o = \rho$; then conservation of mass gives

$$u_i L = u_o l \tag{9.29}$$

Next we equate the kinetic energy gained by the outflowing plasma with the electromagnetic energy flowing into the diffusion regions. The electromagnetic-energy inflow rate per unit area is given by the Poynting flux:

$$|\mathbf{S}| = |\mathbf{E} \times \mathbf{H}| = \frac{EB_i}{\mu_0} = \frac{u_i B_i^2}{\mu_0} \tag{9.30}$$

The mechanical energy out is given by the gain in kinetic energy of the outflowing plasma. The mass flowing in per unit area per unit time, ρu_i, is accelerated to speed ρu_o, so that the rate of energy gain per unit area in the incident flow is

$$\Delta W = \frac{1}{2}\rho u_i (u_o^2 - u_i^2) \tag{9.31}$$

Equating the energy rates in (9.30) and (9.31), and using $u_o \gg u_i$, which follows from (9.29), gives

$$\frac{u_i B_i^2}{\mu_0} = \frac{1}{2}\rho u_i u_o^2 \tag{9.32}$$

so

$$u_o^2 = \frac{2B_i^2}{\mu_0 \rho} = 2v_{Ai}^2 \tag{9.33}$$

where v_{Ai} is the Alfvén velocity in the inflow region. From the magnetic-annihilation calculation we obtained the estimate of l, the thickness of the diffusion region, given in (9.26). Combining this with (9.29) and (9.33) gives us an expression for the inflow speed:

$$u_i^2 = 2^{\frac{1}{2}} v_{Ai}/\mu_0 \sigma L \tag{9.34}$$

so

$$u_i = v_{Ai}(2^{\frac{1}{2}}/R_{mA})^{\frac{1}{2}} \tag{9.35}$$

where

$$R_{mA} = \mu_0 \sigma v_{Ai} L \tag{9.36}$$

What this means is that in all solar-system plasmas for which R_{mA} is very large, the inflow into the reconnection site, which corresponds to the reconnection rate, is very, very slow. Using typical solar-corona parameters, a solar flare would take tens of days to grow, rather than a few minutes as observed. This result, derived independently by Sweet and Parker in the late 1950s, made people tend to rule out reconnection as a viable process.

However, a few years later, Petschek (1964) solved the rate problem by realizing that most of the plasma involved in the reconnection process does not need to flow through the diffusion region in order to be accelerated. Instead, it can be accelerated in the region where MHD is still valid, the so-called convection region. The acceleration occurs as the plasma passes through shock waves that are connected to the diffusion region and that remain fixed in space; that is, they stand in the flow. This process removes the bottleneck caused by requiring that all the

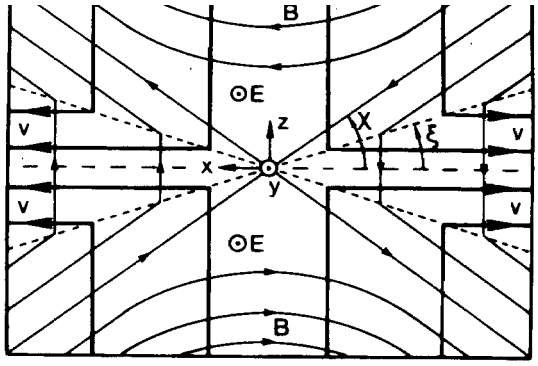

FIG. 9.13. Petschek reconnection geometry. The diffusion region has been shrunk to a dot in the center of the diagram, and the plasma is accelerated at four slow-mode shock waves inclined at angle ξ to the x-axis. (Adapted from Hill, 1975.)

plasma come within a length l of the midplane, and so a much larger inflow rate can be accommodated.

The diffusion region is still important in the sense that the actual process of reconnection must occur there, and so its presence is required, but the diffusion region may now become vanishingly small. The size of the diffusion region will not even enter our calculation. Rather, the entire calculation will be based on jump conditions across an MHD shock. So although at the heart of the process the MHD approximation is being violated, the rate at which reconnection proceeds is based entirely on constraints away from the diffusion region where MHD breaks down, and within the convection region where $\mathbf{E} = -\mathbf{u} \times \mathbf{B}$ holds.

The geometry of this new solution is shown in Figure 9.13. Now the diffusion region has been reduced to a dot at the center of the diagram, and only an insignificant fraction of the flow passes through it. Emanating from this dot are four shock waves shown as dashed lines, at an angle ξ to the x-axis. Both immediately upstream and downstream of these shocks, the magnetic-field and flow vectors are taken as uniform. (Geometric constraints make it impossible for the entire inflow region to be uniform; note that the field lines are curved where they first enter the diagram from top and bottom.) At the shocks, the magnetic field and flow abruptly change in both direction and strength. The magnetic-field strength decreases (field lines are farther apart in the outflow region), and although the flow speed increases (flow lines are closer together in the outflow region), the normal component of the flow velocity drops. These are slow-mode shocks (see Chapter 5), and they are also current sheets. The current is needed both to change the magnetic field and to accelerate the flow via the $\mathbf{j} \times \mathbf{B}$ force. Note also that a parcel of plasma reaches the shock some time after the flux tube it is on has reconnected at the diffusion region; this time delay depends on how far from the diffusion region the plasma crosses the shock.

In the frame of the figure, the shocks are stationary, but in the frame of the plasma the shocks travel along the magnetic field at the inflow Alfvén speed, $v_{Ai} = B_i/(\mu_0 \rho_i)^{\frac{1}{2}}$. We use this to relate the inflow speed u_i to the angle of the shock, ξ, and to the angle between the magnetic field

immediately upstream of the shock and the x-axis, χ. The plasma inflow velocity normal to the shock must equal the shock speed normal to the shock front in the plasma frame for the shock to remain fixed. This gives

$$u_i \cos \xi = v_{Ai} \sin(\chi - \xi) \tag{9.37}$$

Again we can appeal to the steady state and hence require a uniform electric field in the y-direction, equation (9.22). Hence,

$$E_i = u_i B_i \cos \chi = u_o B_o = E_o \tag{9.38}$$

Next, the component of **B** normal to the shock must be conserved. This gives

$$B_i \sin(\chi - \xi) = B_o \cos(\xi) \tag{9.39}$$

Eliminating the magnetic field between (9.38) and (9.39) and using (9.37) gives

$$u_o = \frac{u_i \cos \xi \cos \chi}{\sin(\chi - \xi)} = v_{Ai} \cos \chi \tag{9.40}$$

So, as in the Sweet-Parker solution, the outflow speed is comparable to the inflow Alfvén speed. By conserving mass flow across the shock, we get

$$\rho_i u_i \cos \xi = \rho_o u_o \sin \xi \tag{9.41}$$

where we have now allowed for the plasma to be compressed at the shock (i.e., $\rho_o \geq \rho_i$). Eliminating u_o and u_i between (9.40) and (9.41), after some rearrangement, gives

$$\tan \chi = \frac{\tan \xi}{1 + \rho_o / \rho_i} \tag{9.42}$$

Further rearrangement of (9.40), (9.41), and (9.42) yields an expression for the inflow speed

$$u_i = v_{Ai} \sin \chi / (1 + \rho_i / \rho_o) \tag{9.43}$$

Now, because a slow-mode shock can only compress the plasma, $0 < \rho_i / \rho_o \leq 1$, so

$$\frac{1}{2} \leq u_i / (v_{Ai} \sin \chi) < 1 \tag{9.44}$$

So, in complete contrast to the Sweet-Parker solution, the inflow speed is some reasonable fraction of the inflow Alfvén speed. However, further analysis of the constraints of this solution shows that $u_i \leq 0.1 v_{Ai}$.

Physically the plasma acceleration occurs at the shock fronts and can be pictured as being due to the $\mathbf{j} \times \mathbf{B}$ force. The shock orientation adjusts to accommodate the inflow speed; the outflow speed also varies but remains close to v_{Ai}. This solution so speeds up the allowable reconnec-

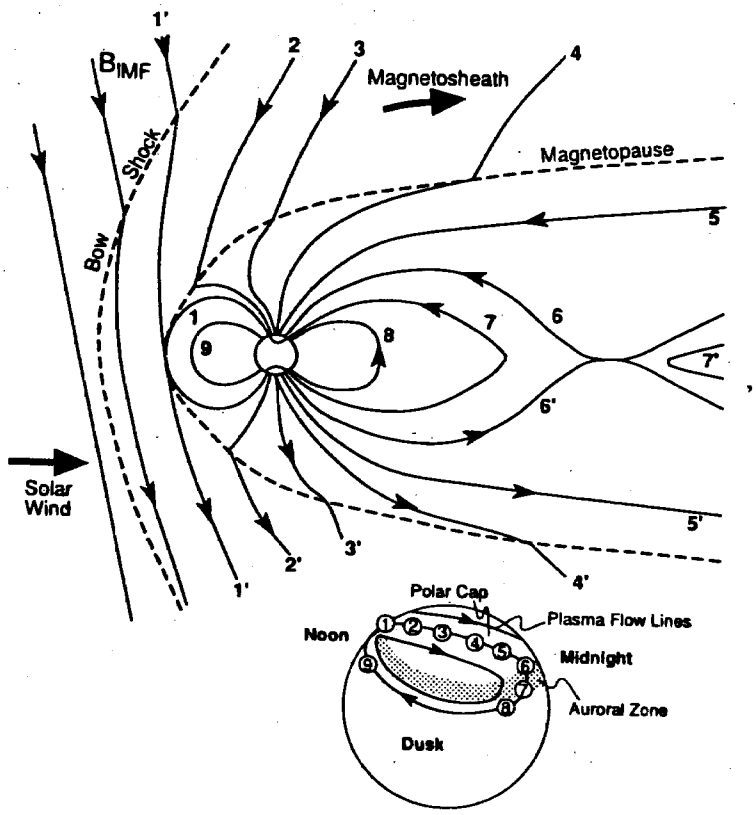

FIG. 9.11. Flow of plasma within the magnetosphere (convection) driven by magnetic reconnection. The numbered field lines show the succession of configurations a geomagnetic field line assumes after reconnection with an IMF field line (1') at the front of the magnetosphere. Field lines 6 and 6' reconnect at a second *x*-line in the tail, after which the field line returns to the dayside at lower latitudes. The inset shows the positions of the feet of the numbered field lines in the northern high-latitude ionosphere and the corresponding high-latitude plasma flows, an antisunward flow in the polar cap, and a return flow at lower latitudes.

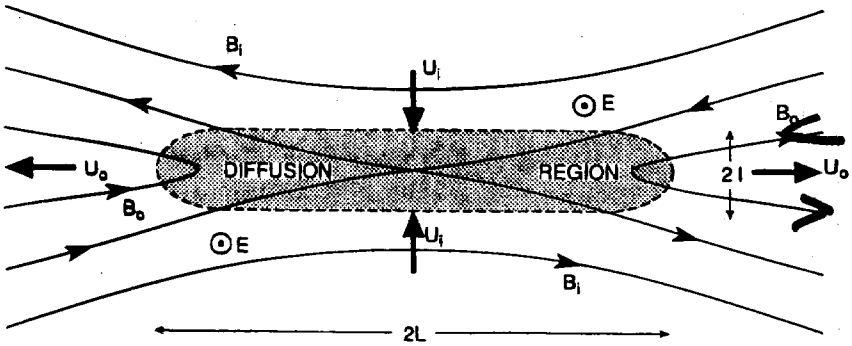

FIG. 9.12. Sweet-Parker reconnection geometry, in which all the reconnecting plasma flows through the shaded diffusion region. Very slow reconnection results.

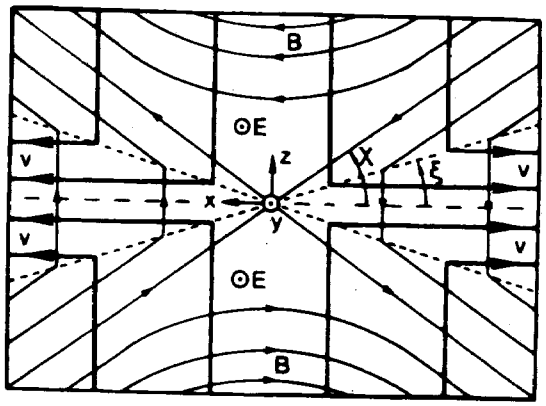

FIG. 9.13. Petschek reconnection geometry. The diffusion region has been shrunk to a dot in the center of the diagram, and the plasma is accelerated at four slow-mode shock waves inclined at angle ξ to the *x*-axis. (Adapted from Hill, 1975.)

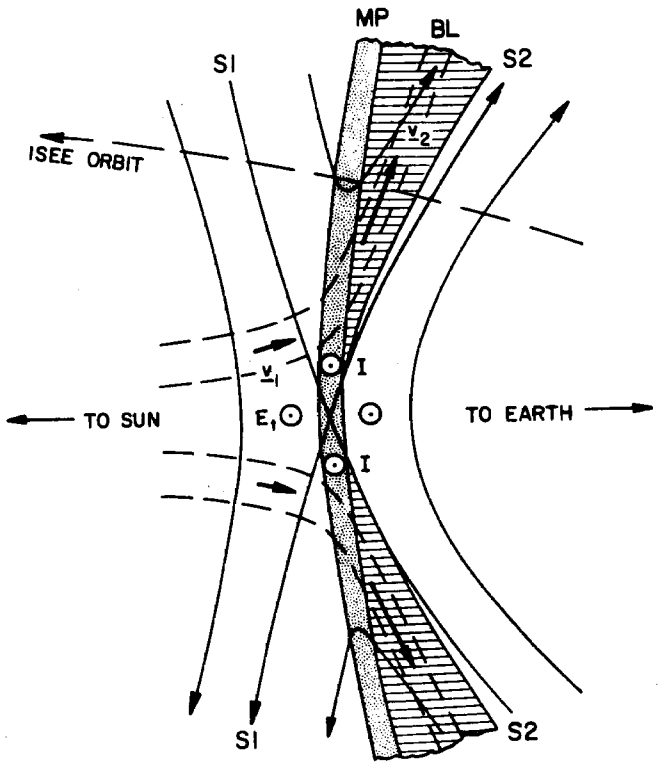

Fig. 4. Meridional view of the reconnection configuration for antiparallel external and internal magnetic fields. The magnetic field lines are shown as solid lines. The magnetopause (MP) is shown as a current layer of finite thickness, with an adjoining boundary layer (BL) of comparable thickness. Those magnetosheath and magnetospheric field lines connected to the separator (or X line) form the outer (S_1) and inner (S_2) separatrices. Dashed lines are stream lines and the heavy arrows indicate plasma flow speed outside and inside the magnetopause. The reconnection electric field, E_t is aligned with the magnetopause current, I. (From Sonnerup et al., 1981).

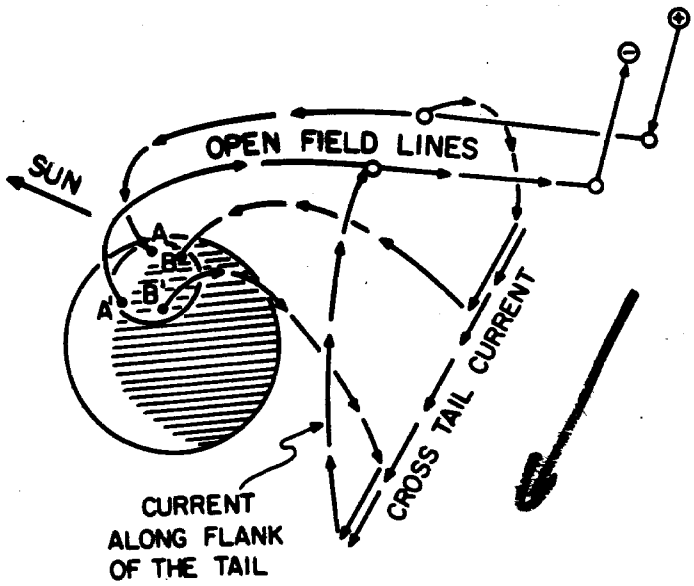

Fig. 7. Schematic view of the way in which region 1 currents may form a shunt of the cross-tail circuit.

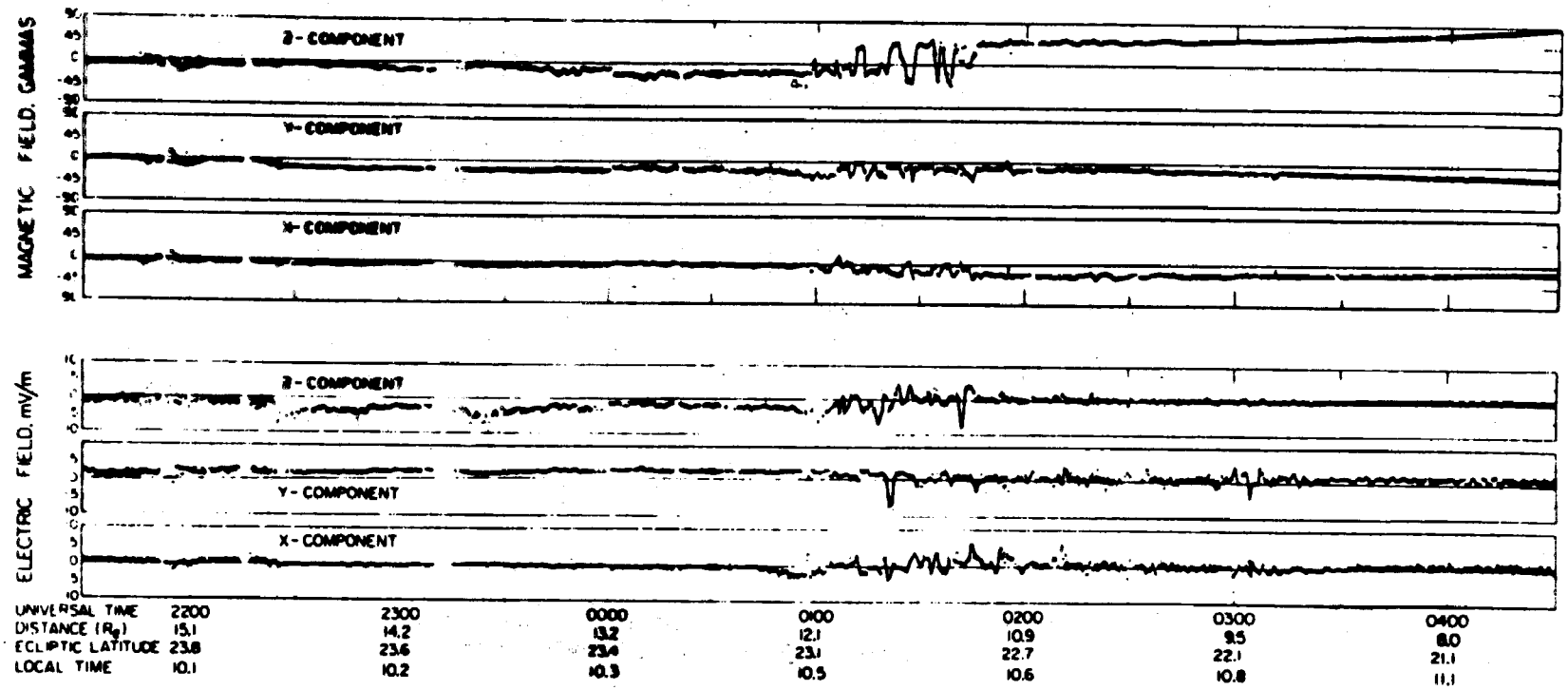

Fig. 1. Seven hours of electric and magnetic field data during which time the ISEE-1 spacecraft passed from the solar wind to the magnetosphere.

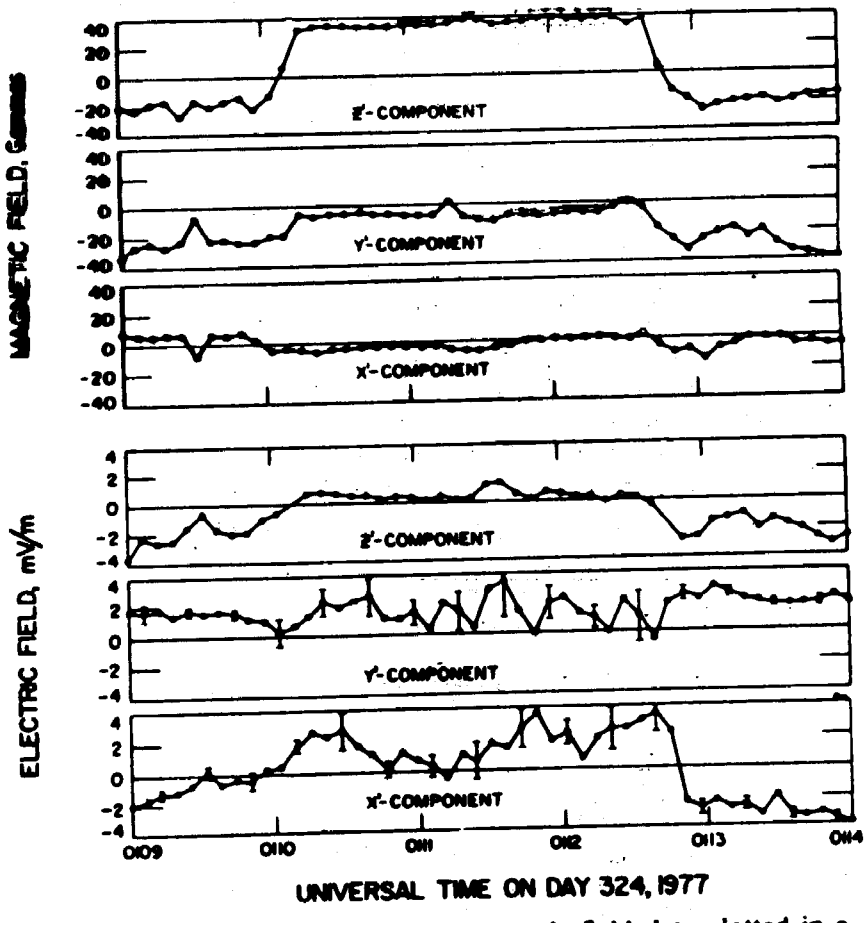
MAGNETIC FIELD, Gamma
40
20
0
-20
-40
Z'-COMPONENT
Y'-COMPONENT
X'-COMPONENT
ELECTRIC FIELD, mV/m
4
2
0
-2
-4
Z'-COMPONENT
Y'-COMPONENT
X'-COMPONENT
0109
0110
0111
0112
0113
0114
UNIVERSAL TIME ON DAY 324, 1977